Interactions of γT273 and γE275 with the β Subunit PSAV Segment that Links the γ Subunit to the Catalytic Site Walker Homology B Aspartate Are Important to the Function of *Escherichia coli* F_1F_o ATP Synthase†

Kathryn W. Boltz and Wayne D. Frasch*

Center for the Study of Early Events in Photosynthesis, Faculty of Biomedicine and Biotechnology, School of Life Sciences, Arizona State University, Tempe, Arizona 85287-4501

Received January 12, 2005; Revised Manuscript Received May 13, 2005

ABSTRACT: In *Escherichia coli* F_1F_o ATP synthase, γT273 mutants that eliminate the ability to form a hydrogen bond to βV265 were incapable of ATP synthase-dependent growth and ATPase-dependent proton pumping, had very low rates of ATPase activity catalyzed by purified F_1, and had significantly decreased sensitivity to inhibition by Mg^{2+}-ADP−AlF_n species, while γT273D and γT273N mutants which maintained or increased the hydrogen bond strength maintained or increased catalytic activity. The βP262G mutation that increases the potential flexibility of the rigid sleeve that surrounds the γ subunit C-terminus also virtually eliminated ATPase activity and susceptibility to Mg^{2+}-ADP−AlF_n inhibition. The γE275 mutants that retained the ability to form the βV265 hydrogen bond had higher ATPase activity than those that eliminated the hydrogen bond. These results provide evidence that the ability to form hydrogen bonds between βV265 and the γ subunit C-terminus contributes significantly to the rate-limiting step of catalysis and to the ability of the F_1F_o ATP synthase to use a proton gradient to drive ATP synthesis. The loss of activity observed with βP262G may result from increased flexibility conferred by glycine that decreases the efficiency of communication between the γ subunit−βV265 hydrogen bonds and the Walker B aspartate at the catalytic site. The partial loss of coupling observed with γT273 mutants that eliminate the βV265 hydrogen bond is consistent with participation of this hydrogen bond in the escapement mechanism for ATP synthesis in which interactions between the γ subunit and $(\alpha\beta)_3$ ring prevent rotation until the empty catalytic site binds substrate.

The F_1F_o ATP synthase consists of the intrinsic membrane protein complex F_o and the extrinsic complex F_1.[1] F_o can use the energy from a transmembrane proton gradient to drive the synthesis of ATP from ADP and inorganic phosphate that is catalyzed by F_1. When F_1 is isolated from F_o and the membrane, it can catalyze the hydrolysis of ATP. The (ADP)(AMPPNP)F_1 crystal structure contains ADP and AMPPNP at the β_{DP} and β_{TP} catalytic sites, while the third catalytic site is empty (β_E) (*1*, *2*). The three α−β subunit heterodimers surround the central γ subunit, with the catalytic sites of the enzyme located on the β subunits at the interfaces with the α subunits. The γ subunit domain that is surrounded by the $(\alpha\beta)_3$ ring forms a coiled coil from the N- and C-terminal α helices.

The γ subunit rotates within the $(\alpha\beta)_3$ ring during catalysis (*3*−*5*). Each of the three catalytic sites on F_1 hydrolyzes ATP sequentially to drive γ subunit rotation (*6*). The binding of Mg^{2+}-ATP to the empty catalytic site initiates a rotation of γ of approximately 80°, while the final 40° rotation occurs upon product release after a 2 ms pause (*7*, *8*). The kinetics of the 2 ms pause are consistent with the presence of two sequential 1 ms steps, suggesting that there are a minimum of five steps during one ATP hydrolysis event (*9*).

The coiled coil within the γ subunit ends with the interaction between the N-terminus and γA263 (MF_1T253)[2] of the C-terminus α-helix (Table 1). The C-terminus α-helix extends beyond the coiled coil by 20 amino acids, of which most are highly conserved (*10*, *11*). This conserved region begins with the arginine and glutamine that interact with the β_E catch loop (*12*), and extends through a sleeve formed by the six α and β subunits. In the β subunit, this sleeve encompasses residues V254 (MF_1V268)−T270 (MF_1T284). The loop and α helix containing βD242 (MF_1D256) and βR246 (MF_1R260) that coordinate the Mg^{2+}-ATP complex (*13*) and bind the ATP γ-phosphate (*14*), respectively, end with residues V254 (MF_1V268)−I261 (MF_1I275) (Figure 1C). First, as these residues exit the α helix, several backbone hydrogen bonds reinforce the V254−I261 structure. Second, residues S263 (MF_1S277)−Q268 (MF_1Q282) comprise a β turn that contains several backbone hydrogen bonds connecting residues S263 (MF_1S277) and A264 (MF_1A278) to residues G266 (MF_1G280)−Q268 (MF_1Q282). These two

† This work was supported by National Institutes of Health Grant GM50202 to W.D.F.

* To whom correspondence should be addressed. E-mail: Frasch@asu.edu. Telephone: (480) 965-8663. Fax: (480) 965-6899.

[1] Abbreviations: F_1, extrinsic membrane-associated protein of the F_1F_o ATP synthase; EF_1, F_1 portion of the *E. coli* F_1F_o ATP synthase; XL10, *E. coli* cell line that includes the γS193C mutation, the six-His tag on the N-terminus of the α subunit, and deletion of an XmnI restriction site.

[2] *E. coli* residue numbering used throughout.

10.1021/bi050070o CCC: $30.25
Published on Web 06/16/2005

Table 1: Comparison of the C-Terminal Region of the γ Subunits from EF_1, Spinach Chloroplast F_1, and Bovine Mitochondrial F_1

strain	residue																			
EF_1	A[a]	R	$_{18}$Q[b]	A	S	$_{15}$I	T	Q	$_{12}$E	L	$_{10}$T	$_{9}$E	I	V	$_{6}$S	G	$_{4}$A	$_{3}$A	A	V	
CF_1	A	$_{20}$R	Q	$_{18}$A	K	$_{16}$I	T	$_{14}$G	E	$_{12}$I	L	$_{10}$E	I	$_{8}$V	A	$_{6}$G	A	N	A	C	V
MF_1	T	R	Q	A	V	I	T	K	E	L	I	E	I	I	S	G	A	A	A	L	D
β_{TP}															●[c]				●		
β_{DP}									●				●								
β_{E}		▲	▲			●	●			●				●							

[a] Residue γA267 in *E. coli* F_1, γA303 in spinach chloroplast F_1, and γT253 in bovine mitochondrial F_1. [b] Subscript numbers indicate the number of residues from the C-terminus. [c] Interactions between the γ subunit and either the hairpin turn of the β subunit (●) or the catch loop of the β subunit (▲) in the (ADP)(AMPPNP)F_1 (*2*) and/or $(ADP{\cdot}AlF_4^-)_2F_1$ (*23*) crystal structure.

rigid structures are bridged by P262 (MF_1P276), the first residue in the βPSAV segment (βP262−βV265).

Many of the interactions between the β subunit sleeve and the γ subunit are hydrophobic (Table 1). As the γ subunit rotates, the sleeve slides up and down the γ subunit such that the β_{TP}PSAV segment is closer to the C-terminus than the other β subunit segments (Figure 1C). Several studies that examined the effects of mutations that truncate various lengths of the C-terminus of the γ subunit have yielded variable results. Deletion of 3−12 amino acids from the C-terminus of the γ subunit did not affect Mg^{2+}-ATPase-dependent rotation of the EF_1 γ subunit as measured by a single-molecule rotation assay (*15*). Although 65−70% of the Mg^{2+}-ATPase activity was retained upon truncation of the C-terminus up to γG282 (MF_1G268), the activity remaining after longer truncations varied from 14 to 80% for comparable truncations between studies (*15*−*17*). In chloroplast F_1, the Ca^{2+}-ATPase activity was ∼150% when the γ subunit was truncated from 6 to 14 residues (*17*).

Single-point mutations in this γ subunit region have had a variety of effects. Some residues have tolerated a loss or reversal of charge or a drastic change in size while maintaining the ability to hydrolyze ATP (*16*). Mutations to other residues of the C-terminal region of the γ subunit have greatly reduced membrane ATPase activity, or ATP synthesis activity as measured by growth on succinate (*18*, *19*). Mutations to γT273 and γE275 decreased membrane ATPase activity, but the effect on succinate growth was variable (*16*, *18*, *19*). These studies suggest that the C-terminus of the γ subunit is important for the function of the F_1 ATPase.

The (ADP)(AMPPNP)F_1 structure that contains ADP and AMPPNP at two of the catalytic sites is likely to represent a low-free energy ground state since it has been derived under a wide variety of conditions (*1*, *2*, 20−22). The $(ADP{\cdot}AlF_4^-)_2F_1$ structure which contains the Mg^{2+}-ADP−fluoroaluminate transition state analogue inhibitor at two catalytic sites, and Mg^{2+}-ADP and SO_4^{2-} at the low-affinity catalytic site, shows distinct conformational differences from the other structures (*23*). The long O−Al−O bond lengths and the presence of four fluorines of the bound fluoroaluminate suggest that $(ADP{\cdot}AlF_4^-)_2F_1$ may represent a post-transition state intermediate conformation. In this latter structure, the γ subunit coiled coil is more tightly wound, and the α−β domain of the γ subunit is rotated ∼20° relative to the ground state structures. Although β_EV265 in the PSAV segment forms a hydrogen bond with γT273 in both structures, β_{DP}V265 forms a hydrogen bond with γE275 only in $(ADP{\cdot}AlF_4^-)_2F_1$ (Figure 1B).

It has been proposed that intersubunit hydrogen bonds between the γ subunit and the $(\alpha\beta)_3$ ring prevent rotation driven by the proton gradient until the empty catalytic site binds substrate (*12*, *24*). Deformation of the catch loop−γ subunit interactions induced by substrate binding would provide an escapement mechanism that would maintain tight coupling between the proton-motive force and ATP synthesis. Presumably, in addition to the catch loop, the hydrogen bonds and salt bridges that contribute to the escapement mechanism are located in other regions that connect γ to the $(\alpha\beta)_3$ ring. We now report the analysis of the effects of mutations that either eliminate the hydrogen bonds between the C-terminus of the γ subunit and the PSAV segment of the β subunits or mutate βP262 to allow the PSAV segment to be more mobile. The results indicate that the hydrogen bond between β_EV265 and γT273 is very important for both ATP synthesis and hydrolysis, while the hydrogen bond between β_{DP}V265 and γE275 is important for ATP hydrolysis. The increased mobility allowed by the βP262G mutation affected both ATP synthesis and hydrolysis, suggesting that the rigidity of the PSAV segment is important for catalysis.

EXPERIMENTAL PROCEDURES

Strains and Plasmids. The parent plasmid and *E. coli* strain used in the this study are the same as those described previously (*12*). All site-directed mutagenesis for the current study was performed in plasmid pXL1 using XL Quick Change Kit (Stratagene). The oligonucleotide primers for the creation of each mutant are shown in Table 2. The F_1 ATPase in the XL10 strain of *E. coli* contains a six-His tag on the α subunit and γS193C mutation as described previously (*12*). Methods for culture growth and purification of EF_1 were employed by following the method of Greene and Frasch (*12*). Growth yield in limiting glucose was measured through a modification of the procedure of Senior et al. (*25*). Growth of strains in 1 L volumes of TDA with 3 mM glucose was followed through hourly optical density measurements. Reported values were based on the maximum optical density at 600 nm attained.

The rate of ATP hydrolysis was determined using an ATP-regenerating coupled assay that consisted of 50 mM Tris-HCl (pH 8.0), 10 mM KCl, 2.5 mM phosphoenolpyruvate, 0.15−0.3 mM NADH, 50 μg/mL pyruvate kinase, 50 μg/mL lactic dehydrogenase, and 3 nM F_1, with 2 mM Mg^{2+}-ATP. The rate was determined as a change in absorbance at 340 nm using a Cary 100 Bio UV−vis spectrophotometer (Varian) equipped with a stir-controlled Peltier device. The reaction was initiated by the addition of F_1 to the assay mixture. Reaction rates were calculated from data collected 6−8 min after initiation of the reaction to allow for dissociation of the ϵ subunit and to minimize inhibition by entrapped Mg^{2+}-ADP (*26*). To minimize entrapped Mg^{2+}-

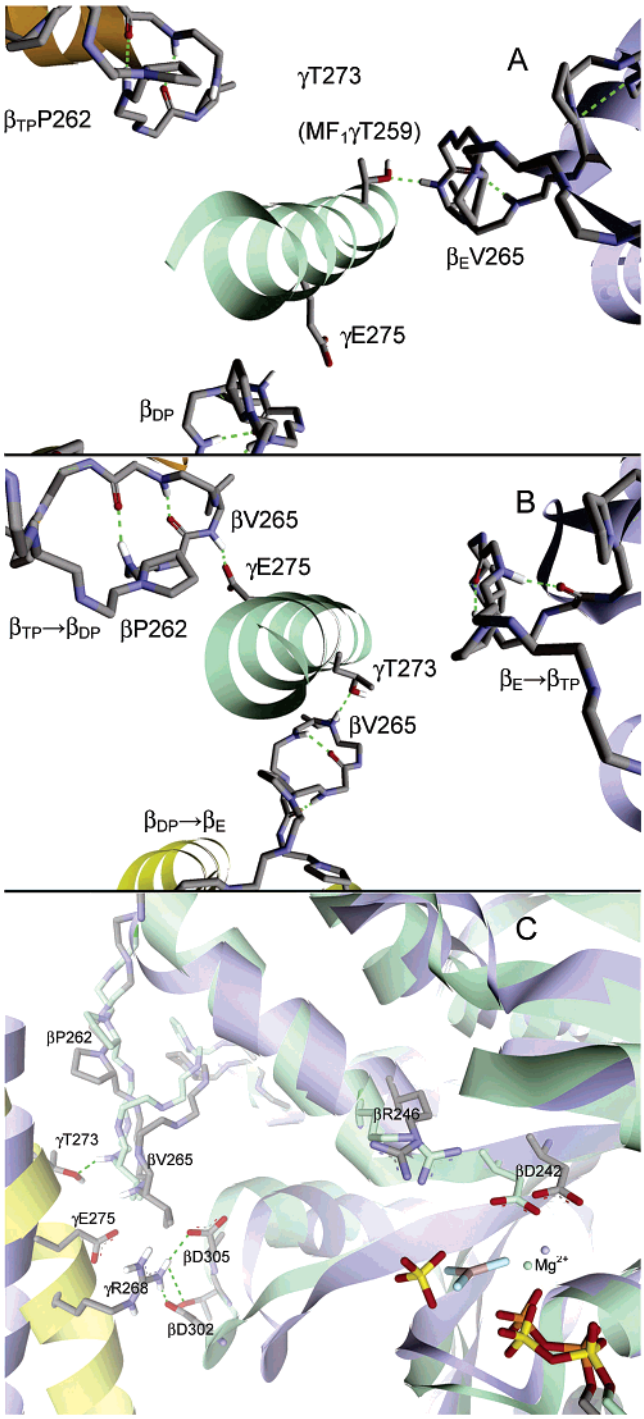

FIGURE 1: Interactions between the γ subunit and the β subunit rigid sleeve which includes the βPSAV segment. (A) (ADP)-(AMPPNP)F_1 structure (*2*) that shows the hydrogen bond between γT273 and β_EV265. (B) (ADP·AlF_4^-)$_2F_1$ structure (*23*) that shows the hydrogen bonds between γT273 and β_EV265 and between γE275 and β_{DP}V265. The orientation of the protein complex in panel B is consistent with the 100° rotation from panel A that would occur during a catalytic step. Hydrogen bonds and prolines which strengthen the rigid sleeve of the β subunit which includes the βPSAV segment are shown. (C) Superposition of the (ADP·AlF_4^-)$_2F_1$ (*23*) and (ADP·AlF_3)(AMPPNP)F_1 (*2*) structures aligned through the Magic Fit function of the DeepView/Swiss-PDB Viewer (*44*): blue for the (ADP·AlF_3)(AMPPNP)F_1 β_{DP} subunit, γ subunit, Mg^{2+}, and AlF_3, green for the (ADP·AlF_4^-)$_2F_1$ β_E subunit and Mg^{2+}, and yellow for the (ADP·AlF_4^-)$_2F_1$ γ subunit, ADP, and SO_4^{2-}. Images are reproduced from Protein Data Bank files using WebLab ViewerLite by Accelrys.

ADP further, preparations of F_1 were stored in 1 mM Mg^{2+}-ATP, and diluted 50-fold in the reaction mixture upon initiation of the ATPase assay.

The effects of the addition of $AlCl_3$ and NaF to F_1 containing Mg-ADP in a single catalytic site were determined using a procedure modified from that of Dou et al. (*27*). Isolated F_1 was incubated with equimolar ADP and 2 mM $MgCl_2$ for 1 h. Then, 50 μM $AlCl_3$ and 10 mM NaF were added to an aliquot of the incubated mixture. The reaction mixtures were incubated at room temperature. At the indicated times, 50 μL samples were assayed at 25 °C using the ATP-regenerating system described above.

Activation energies and entropic and enthalpic components of the transition state for multisite ATP hydrolysis were calculated from measurements of maximal rates of ATPase activities as a function of temperature as described using eqs 1−3 (*28*):

$$E_A = \Delta H^{\ddagger} + RT \quad (1)$$

$$\Delta G^{\ddagger} = \Delta H^{\ddagger} - T\Delta S^{\ddagger} \quad (2)$$

$$\Delta G^{\ddagger} = -RT \ln(Nh/RTk_{cat}) \quad (3)$$

where k_{cat} is the turnover number, T is the temperature, E_A is the Arrhenius activation energy, N is Avogadro's number, and $\Delta H^{\ddagger}$ and $\Delta S^{\ddagger}$ are the enthalpic and entropic components, respectively, of the changes in Gibbs free energy of activation ($\Delta G^{\ddagger}$).

Membrane vesicles were prepared through a modification of the procedure of Futai et al. (*29*). Logarithmic phase cells were passed through a French press at 14 000 psi, and the mixture was centrifuged at 35000*g* for 10 min. The collected supernatant was ultracentrifuged at 200000*g* for 30 min. The pelleted membranes were resuspended at 100 mg/mL in 50 mM Tris-HCl and 2 mM $MgCl_2$ (pH 8.0).

Formation of an electrochemical gradient was followed by suspending membrane vesicles in 2 mL of 50 mM Tris-HCl, 2 mM $MgCl_2$, 140 mM KCl, 1 μg/mL valinomycin, and 1 μM acridine orange (pH 8.0). The fluorescence at 530 nm (excitation at 490 nm) was monitored at room temperature with a stirred cuvette in a SPEX FluoroMax fluorometer. Fluorescence quenching was initiated by the addition of either 2 mM lactate to 10 mg of membranes or 2 mM ATP to 100 mg of membranes. The transmembrane proton gradient was collapsed by the addition of 2 μM carbonylcyanide-*m*-chlorophenylhydrazone (CCCP).

RESULTS

The relative abilities of the mutants to grow via oxidative phosphorylation on minimal medium in the presence of either succinate or limiting glucose were determined. The ability of these strains to grow was compared to that of XL10, which was used as the wild-type strain, and to that of AN887 (*30*), which does not express the enzyme due to a Mu phage suppression of the endogenous unc operon. Table 3 summarizes doubling times from growth on succinate, and maximum optical density obtained when growth occurred on 3 mM glucose. Growth on succinate and on minimal glucose yielded similar results in all cases. The extent of growth of the βP262G mutant strain on succinate and limiting glucose was reduced by ~2-fold. The βP262A strain had

Table 2: Primers Used To Generate Mutant Strains[a]

mutant strain	mutagenic primer
βP262G	5′-GCACTGCTGGGCCGTATG**GG**TTCAGCGGTAGGTTATCAGCCG-3′
βP262A	5′-GCACTGCTGGGCCGTATG**G**CTTCAGCGGTAGGTTATCAGCCG-3′
γT273A	5′-CGTCAGGCCAGCATT**G**CTCAGGAACTCACCGAG-3′
γT273V	5′-GCTCGTCAGGCCAGCATT**GT**TCAGGAACTCACCGAG-3′
γT273D	5′-CGTCAGGCCAGCATT**GA**TCAGGAACTCACCGAG-3′
γT273N	5′-CGTCAGGCCAGCATTA**A**TCAGGAACTCACCGAG-3′
γT273H	5′-CGTCAGGCCAGCATT**CA**TCAGGAACTCACCGAG-3′
γE275A	5′-GCCAGCATTACTCAGG**C**ACTCACCGAGATCGTC-3′
γE275V	5′-CAGGCCAGCATTACTCAGG**T**ACTCACCGAGATCGTC-3′
γE275L	5′-CAGGCCAGCATTACTCAG**CT**ACTCACCGAGATCGTC-3′
γE275G	5′-GCCAGCATTACTCAGG**G**ACTCACCGAGATCGTC-3′
γE275D	5′-GCCAGCATTACTCAGGA**T**CTCACCGAGATCGTC-3′
γE275H	5′-GCCAGCATTACTCAG**C**A**C**CTCACCGAGATCGTC-3′

[a] Codons containing changes are indicated with bold underlined text. Complementary primers (not shown) were also used in each mutagenesis reaction.

Table 3: Comparison of the Relative Ability of XL10 and Mutant Strains To Grow via Oxidative Phosphorylation Utilizing Succinate as the Sole Carbon Source, Growth Yield in Limiting Glucose, and Purified EF_1 ATPase To Hydrolyze ATP at 2 mM Mg-ATP at 25 °C

strain	succinate-dependent doubling time (h)	succinate-dependent growth rate (% of that of XL10[b])	growth yield in limiting glucose (% of that of XL10)	k_{cat} ATPase (25 °C)	k_{cat} (% of that of XL10)
XL10	2.39	100	100	115	100
AN887	—[a]	0	60	nd[c]	nd[c]
βP262G	3.88	62	81	3	3
βP262A	2.52	95	99	120	104
γT273A	—[a]	0	60	1	1
γT273V	—[a]	5	64	2	2
γT273D	1.94	123	100	190	165
γT273N	3.23	74	94	31	27
γT273H	—[a]	0	60	5	4
γE275A	2.06	116	97	36	31
γE275V	2.02	118	100	57	50
γE275L	3.37	71	98	57	50
γE275G	2.21	108	106	39	34
γE275D	3.23	74	98	78	68
γE275H	2.39	100	93	86	75

[a] Culture did not double over the course of a 12 h period. [b] Measured as the slope at log phase. [c] Not determined.

ATP synthase-dependent growth similar to that of XL10. Hydrophobic mutations γT273A and γT273V did not grow on succinate or minimal glucose, suggesting that this residue is very important for ATP synthase activity. Charged mutation γT273D had ATP synthase-dependent growth comparable to that of XL10. Polar mutation γT273N also had ATP synthase-dependent growth comparable to that of XL10, though polar mutation γT273H did not grow on these media. None of the hydrophobic, polar, or charged mutations of γE275 affected succinate or limiting glucose growth significantly. This suggests that γE275 is not important for ATP synthesis.

The F_1 ATPase was purified from *E. coli* grown to late log phase on media containing 30 mM glucose. The F_1 ATPase isolated from all *E. coli* mutants grown in this manner contained all five subunits ($\alpha\beta\gamma\delta\epsilon$) as determined by SDS−PAGE (data not shown). These results indicate that the mutations did not significantly affect the synthesis and assembly of the enzyme.

Mutant membranes were examined for the ability to generate a proton-motive force from lactate via electron transport (Table 4). The extent of quenching observed with βP262G was 85% of that of XL10, while βP262A was similar to XL10. Hydrophobic mutations γT273A and γT273V both decreased the extent of lactate-induced fluorescence quenching to approximately half of the extent of XL10 quenching, suggesting that these mutations weakened the coupling of these membranes. Charged and polar mutations γT273D, γT273N, and γT273H decreased the level of lactate-induced fluorescence quenching to 85, 85,

Table 4: Comparison of Electrochemical Gradient Formation in Membranes from XL10 and Mutant Strains Measured by Fluorescence Quenching of Acridine Orange

strain	lactate-induced $\Delta\mu_H^+$ (%)[a]	ATP-induced $\Delta\mu_H^+$ (%)
XL10	100	100
βP262G	85	0
βP262A	103	32
γT273A	50	0
γT273V	58	0
γT273D	85	152
γT273N	85	42
γT273H	74	27
γE275A	84	91
γE275V	90	51
γE275L	94	55
γE275G	90	132
γE275D	106	209
γE275H	83	95

[a] The level of quenching was calculated by taking the difference between the maximum level of fluorescence quenching after the addition of lactate or ATP and the level after addition of 2 μM CCCP and then dividing by the value obtained for XL10 membranes (see Figure 2).

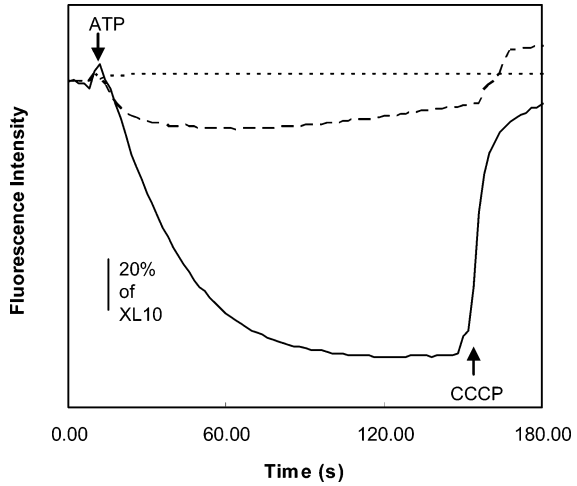

FIGURE 2: Formation of an ATP-dependent electrochemical gradient of protons measured by fluorescence quenching of acridine orange in membrane vesicles from strains XL10 (—), βP262A (− − −), and βP262G (- - -).

and 74% of that of XL10, respectively. The extent of quenching observed with hydrophobic mutations to γE275 was 84−94%, while that for γE275G was 90% of that of XL10. Charged and polar mutations γE275D and γE275H quenched at levels that were 106 and 83% of that of XL10, respectively.

Figure 2 shows the effects of the βP262 mutations on ATP-dependent proton pumping as measured by fluorescence quenching of acridine orange. The strain containing βP262G was incapable of forming a proton gradient upon addition of ATP, while the level of quenching observed with the βP262A strain was 32% of that of XL10. The extent of ATP-dependent fluorescence quenching observed for all strains is summarized in Table 4. Membranes isolated from strains that contain hydrophobic mutations γT273A and γT273V were unable to pump protons driven by ATP. Charged mutation γT273D increased the level of ATP-dependent fluorescence quenching to 152% of that of XL10, while polar mutations γT273N and γT273H decreased the level of quenching to 42 and 27%, respectively. Hydrophobic mutations γE275A, γE275V, and γE275L decreased the level of ATPase-induced quenching to 91, 51, and 55% of that of XL10, respectively, while γE275G increased it to 132% of the level of quenching of XL10. Charged mutation γE275D increased the level of ATP-dependent fluorescence quenching to 209% of that of XL10, while the level of quenching observed with polar mutation γE275H was 95% of that of XL10.

Arrhenius plots of the Mg^{2+}-ATPase activity catalyzed by purified F_1-ATPase are shown in panels A and B of Figure 3. With the exceptions of the mutations to βP262 and γT273H, the Arrhenius plots remained linear up to 45 °C. Mutations βP262G, βP262A, and γT273H were stable to 25, 32.5, and 30 °C, respectively, and thus, a direct comparison of the effects of the mutations on k_{cat} was made at 25 °C (Table 3). Mutation βP262G decreased the k_{cat} to 3% of that of XL10, while mutation βP262A had little effect on the k_{cat}.

Hydrophobic mutations γT273A and γT273V decreased k_{cat} to 1−2% of the XL10 k_{cat}. Charged mutation γT273D increased k_{cat} to 165% of the XL10 rate, while polar mutations γT273N and γT273H decreased k_{cat} to 27 and 4%

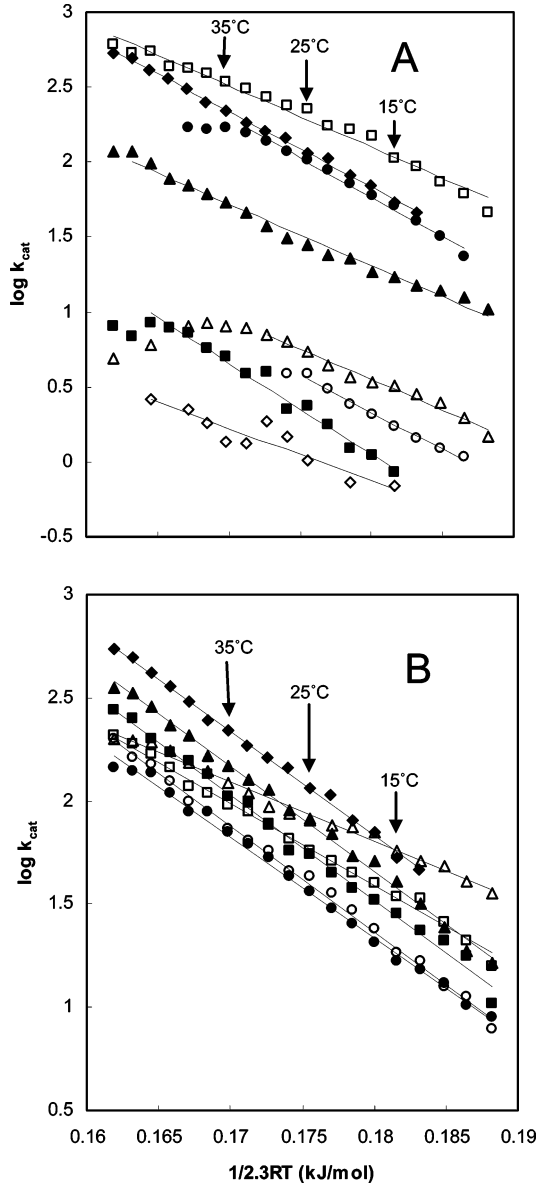

FIGURE 3: Arrhenius analysis of Mg-ATPase activity catalyzed by purified soluble F_1. (A) XL10-F_1 (◆), βP262G-F_1 (○), βP262A-F_1 (●), γT273A-F_1 (◇), γT273V-F_1 (■), γT273D-F_1 (□), γT273N-F_1 (▲), and γT273H-F_1 (△). (B) XL10-F_1 (◆), γE275A-F_1 (●), γE275V-F_1 (■), γE275L-F_1 (□), γE275G-F_1 (○), γE275D-F_1 (▲), and γE275H-F_1 (△). Data points represent mean values from multiple analyses of each strain. Linear relations were generated by least-squares regression analysis of the data.

of the XL10 rate, respectively. Hydrophobic mutations γE275A, γE275V, and γE275L decreased k_{cat} to 31, 50, and 50% of the XL10 rate, respectively, and γE275G decreased k_{cat} to 34% of the XL10 rate. The k_{cat} values of charged and polar mutations γE275D and γE275H were 68 and 75% of the XL10 rate, respectively.

The isokinetic relationship of the mutants is shown in Figure 4. For any single type of chemical reaction, a linear free energy relationship exists between the log(k_{cat}) at two different temperatures. Thus, log plots that compare activities at different temperatures can determine if reactions have a similar rate-limiting step (*31*, *32*). The linear dependence observed with the mutants in Figure 4 suggests that the enzymes containing these mutations all have a similar rate-limiting step. Together, these points represent a continuum

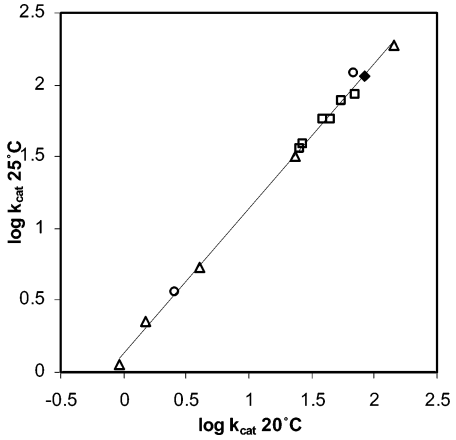

FIGURE 4: Isokinetic correlations of log k_{cat} at 20 °C vs log k_{cat} at 25 °C catalyzed by F_1 solubilized from XL10 (◆), βP262 strains (○), γT273 strains (△), and γE275 strains (□).

Table 5: Comparison of Thermodynamic Values at 25 °C for Mg^{2+}-ATP Hydrolysis Catalyzed by F_1 Isolated from XL10 and Mutants

strain	E_a (kJ/mol)	$\Delta H^{\ddagger}$ (kJ/mol)	$T\Delta S^{\ddagger}$ (kJ/mol)	$\Delta G^{\ddagger}$ (kJ/mol)
XL10	54.5	52.0	−9.2	61.2
βP262A	52.6	50.1	−11.0	61.1
βP262G	50.3	47.8	−22.0	69.8
γT273A	29.6	27.1	−45.5	72.7
γT273V	60.7	58.2	−12.7	70.9
γT273D	42.9	40.4	−19.6	60.0
γT273N	41.3	38.8	−25.6	64.4
γT273H	30.5	28.0	−40.8	68.8
γE275A	49.3	46.8	−17.3	64.1
γE275V	51.2	48.7	−14.2	62.9
γE275L	40.1	37.6	−25.3	62.9
γE275G	53.1	50.6	−13.3	63.9
γE275D	51.3	48.8	−13.4	62.2
γE275H	30.2	27.8	−34.2	62.0

in which changes in structure affect the energy of the rate-limiting step.

From the slopes of the Arrhenius plots indicated by the solid lines in Figure 3, the values for enthalpy, entropy, and free energy of activation were calculated using eqs 1−3 at 25 °C (Table 5). The $\Delta G^{\ddagger}$ of XL10 at this temperature is 61.2 kJ/mol. Because the free energy of activation, $\Delta G^{\ddagger}$, is inversely proportional to k_{cat}, a k_{cat} value equivalent to that of XL10 can result from any combination of $\Delta H^{\ddagger}$ and $\Delta S^{\ddagger}$ due to eq 2 and the enthalpy−entropy compensation effect. Isobars representing the indicated percentage of the k_{cat} value of XL10 (Figure 5) were derived from the inverse relationship between k_{cat} and $\Delta G^{\ddagger}$. The βP262G mutant decreased $\Delta H^{\ddagger}$ by only 4.2 kJ/mol, while $T\Delta S^{\ddagger}$ decreased it by 12.8 kJ/mol, consistent with the possibility that the glycine allows a significant increase in the flexibility in the rigid sleeve. The increase in $\Delta H^{\ddagger}$ of 1.8 kJ/mol caused by the βP262A mutation was compensated by the decrease in $T\Delta S^{\ddagger}$ of 1.9 kJ/mol relative to that of XL10.

With the exception of γT273V, mutations to γT273 decreased $\Delta H^{\ddagger}$ and decreased $T\Delta S^{\ddagger}$ relative to those of XL10. Hydrophobic mutation γT273V increased $\Delta H^{\ddagger}$ by 6.2 kJ/mol yet only decreased $T\Delta S^{\ddagger}$ by 3.5 kJ/mol relative to those of XL10. Although hydrophobic mutation γT273A produced a large decrease in $\Delta H^{\ddagger}$ (24.9 kJ/mol), the larger decrease in $T\Delta S^{\ddagger}$ (36.3 kJ/mol) resulted in the low observed ATPase activity. The increase in the k_{cat} of γT273D relative to that

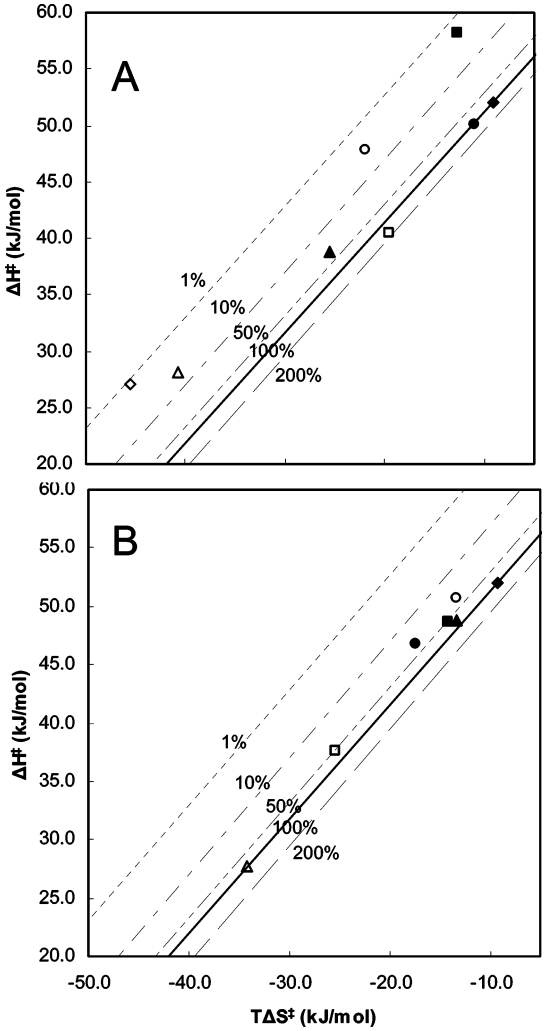

FIGURE 5: Free energy plot of Mg-ATPase activity catalyzed by soluble F_1. Values for $\Delta H^{\ddagger}$, $T\Delta S^{\ddagger}$, and $\Delta G^{\ddagger}$ were derived at 25 °C from the Arrhenius data in Figure 3. (A) XL10-F_1 (◆), βP262G-F_1 (○), βP262A-F_1 (●), γT273A-F_1 (◇), γT273V-F_1 (■), γT273D-F_1 (□), γT273N-F_1 (▲), and γT273H-F_1 (△). (B) XL10-F_1 (◆), γE275A-F_1 (●), γE275V-F_1 (■), γE275L-F_1 (□), γE275G-F_1 (○), γE275D-F_1 (▲), and γE275H-F_1 (△). Isobars for $\Delta G^{\ddagger}$ are shown as lines that are the percentages of the indicated XL-10 k_{cat} values.

of XL10 resulted from a decrease in $\Delta H^{\ddagger}$ of 11.6 kJ/mol, accompanied by a smaller $T\Delta S^{\ddagger}$ decrease (10.4 kJ/mol). Of the polar mutations, γT273H produced a larger decrease in $\Delta H^{\ddagger}$ (24.0 kJ/mol) than γT273N (13.2 kJ/mol) compared to XL10. The much larger decrease in $T\Delta S^{\ddagger}$ observed with γT273H (31.6 kJ/mol) than with γT273N (16.4 kJ/mol) resulted in the lower activity of the former mutant.

All mutations of γE275 decreased both $\Delta H^{\ddagger}$ and $T\Delta S^{\ddagger}$. Hydrophobic mutations γE275A, γE275V, and γE275L decreased $\Delta H^{\ddagger}$ by 5.2, 3.3, and 14.4 kJ/mol relative to that of XL10, respectively, while the $T\Delta S^{\ddagger}$ values compensated by decreasing by 8.1, 5.0, and 16.1 kJ/mol relative to that of XL10, respectively. Substitution γE275G decreased $\Delta H^{\ddagger}$ by 1.4 kJ/mol and decreased $T\Delta S^{\ddagger}$ by 4.1 kJ/mol compared to those of XL10. For the four mutants described above, the loss of activity was due to a smaller enthalpic than entropic effect. Charged mutation γE275D produced a modest decrease in $\Delta H^{\ddagger}$ of 3.2 kJ/mol, which was compensated by a decrease in $T\Delta S^{\ddagger}$ of 4.2 kJ/mol relative to that of XL10. Large changes in both $\Delta H^{\ddagger}$ and $T\Delta S^{\ddagger}$ were observed with

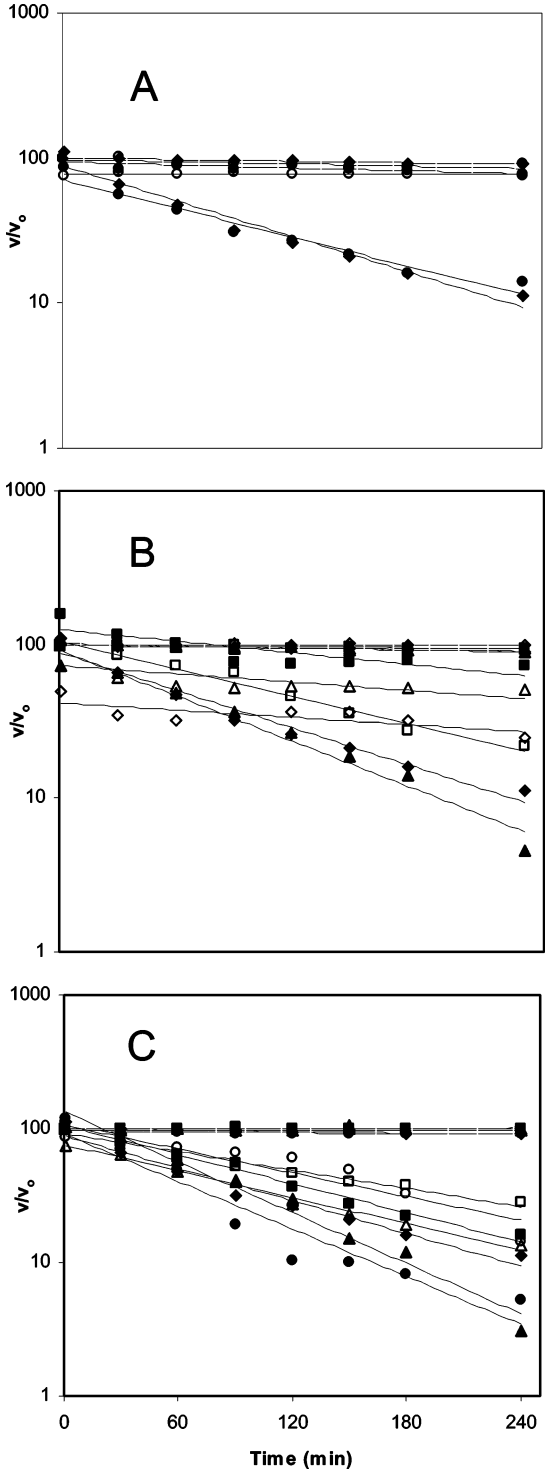

FIGURE 6: Inhibition by Mg^{2+}-ADP (dashed lines), and with fluoroaluminate (solid lines) of Mg^{2+}-ATPase activity catalyzed by soluble F_1 at the indicated times. (A) XL10-F_1 (◆), βP262G-F_1 (○), and βP262A-F_1 (●). (B) XL10-F_1 (◆), γT273A-F_1 (◇), γT273V-F_1 (■), γT273D-F_1 (□), γT273N-F_1 (▲), and γT273H-F_1 (△). (C) XL10-F_1 (◆), γE275A-F_1 (●), γE275V-F_1 (■), γE275L-F_1 (□), γE275G-F_1 (○), γE275D-F_1 (▲), and γE275H-F_1 (△). The rate v_o is the rate of a sample containing Mg-ADP in one catalytic site, but in the absence of Al^{3+} and F^-. The rate v is the rate at the indicated time after adding Al^{3+} and F^- to a sample containing Mg-ADP in one catalytic site.

polar mutation γE275H in a manner similar to that for the γT273H mutant. However, since these changes almost completely compensated each other ($\Delta\Delta H^{\ddagger} = 24.2$ kJ/mol, $\Delta T\Delta S^{\ddagger} = -25.0$ kJ/mol), k_{cat} was 75% of the rate of XL10.

Table 6: Comparison of the Rates of Formation of the Mg^{2+}-ADP−Fluoroaluminate Complexes Catalyzed by the Isolated F_1

strain	k_{inact} (min^{-1})	% of that of XL10
XL10	9.4×10^{-3}	100
βP262G	0.01×10^{-3}	0.1
βP262A	7.6×10^{-3}	81
γT273A	1.8×10^{-3}	19
γT273V	2.9×10^{-3}	31
γT273D	6.8×10^{-3}	72
γT273N	11.3×10^{-3}	120
γT273H	2.1×10^{-3}	22
γE275A	16.2×10^{-3}	172
γE275V	8.4×10^{-3}	89
γE275L	5.3×10^{-3}	56
γE275G	11.3×10^{-3}	120
γE275D	14.6×10^{-3}	155
γE275H	7.6×10^{-3}	81

A tightly bound inhibitory complex forms between F_1 and the Mg^{2+}-ADP−AlF_n species (*27*, *33*, *34*). Figure 6 shows the loss of ATPase activity as a function of time when F_1 was incubated with equimolar ADP and 2 mM $MgCl_2$ for 1 h followed by addition of 50 μM $AlCl_3$ and 10 mM NaF. The rates of inactivation approximated first-order processes. The first-order rate constants for the mutants are summarized in Table 6. Formation of the inhibitory Mg^{2+}-ADP−fluoroaluminate complex occurred at a much slower rate with βP262G-F_1 (0.1%) than with βP262A-F_1 (81%) or XL10-F_1 (100%).

The rate of formation of this inhibitory complex was also substantially slower with mutations γT273A, γT273V, and γT273H. If one ignores the zero time points for these mutants, it appears that the Mg^{2+}-ADP−fluoroaluminate complexes form extremely slowly, if at all, in a single catalytic site. Therefore, it can be argued that the substitution of γT273 with alanine, valine, or histidine not only prevents ATP hydrolysis but also prevents formation of the Mg^{2+}-ADP−fluoroaluminate complex in a single catalytic site. The deviations in the zero time values result from the low ATPase activity of the mutant in the absence of inhibitor. Charged and polar mutations γT273D (72%) and γT273N (120%) were most susceptible to the inhibitory Mg^{2+}-ADP−fluoroaluminate complex. The rates of inactivation by the inhibitory Mg^{2+}-ADP−fluoroaluminate complex for hydrophobic mutations γE275A, γE275V, and γE275L were 172, 89, and 56%, respectively, of the XL10 inactivation rate, while γE275G increased the rate of inactivation to 120% of the XL10 rate. The rates of inactivation of charged and polar mutations γE275D and γE275H were 155 and 81%, respectively, of the XL10 rate.

DISCUSSION

In bovine mitochondrial F_1 structures (*1*, *2*, *20*, *23*, *35*, *36*), the hydroxyl group of γT273 (MF_1T259) forms a hydrogen bond to the β subunit PSAV segment via the backbone amide of β_EV265 (MF_1V279) (Figure 1A). In the $(ADP{\cdot}AlF_4^-)_2F_1$ structure, a hydrogen bond exists between γE275 (MF_1E261) and β_{DP}V265 (MF_1V279) in addition to the γT273−β_EV265 hydrogen bond (Figure 1B). The Walker homology B aspartate [βD242 (MF_1D256)] and βR246 (MF_1-R260) that bind the Mg^{2+} cofactor and phosphate connect through a short α helix to the rigid sleeve that includes the PSAV segment. If the $(ADP{\cdot}AlF_4^-)_2F_1$ structure represents

a rate-limiting intermediate state that forms upon a Mg^{2+}-ATPase-induced 100° rotation of the γ subunit from the ground state, then the γT273−β_EV265 ground state hydrogen bond would be broken upon rotation which moves γT273 into contact with β_{DP}V265, at which time the $\beta_{DP} \rightarrow \beta_E$ conformational change is initiated (Figure 1A → Figure 1B). In the course of the $\beta_{DP} \rightarrow \beta_E$ conformational change, the affinity of Mg^{2+}-ADP at the catalytic site decreases (*37*) which includes the dissociation of the Walker homology B aspartate from the coordination sphere of the bound metal (*13*, *38*−*41*) to promote product release.

The effects of γT273 mutations reported here are consistent with the involvement of the γT273−β_EV265 hydrogen bond in the $\beta_{DP} \rightarrow \beta_E$ conformational changes. Hydrophobic mutations γT273A and γT273V that eliminate the hydrogen bond resulted in a 2 order of magnitude loss of both ATP synthesis and hydrolysis activity, and decreased the susceptibility to inhibition by the Mg^{2+}-ADP−AlF_n complex. The decrease in the level of ATPase-dependent proton pumping reported here that resulted from γT273V is somewhat larger than that previously observed (*16*, *18*). This difference is likely to have resulted from the presence of the α subunit six-His tag and γS193C mutations that are also incorporated into the enzyme in the strains used here. The γT273G mutant (*16*, *18*), which cannot form a hydrogen bond, also causes a decrease in the level of ATPase-dependent fluorescence quenching and membrane ATPase activity.

Mutations γT273D and γT273N that retained the ability to form the γT273−β_EV265 hydrogen bond also retained both ATP synthase and hydrolysis activity, and were more susceptible to Mg^{2+}-ADP−AlF_n inhibition than the hydrophobic mutations. In fact, the γT273D mutation to provide a formal negative charge at that position, and thus a significantly stronger hydrogen bond to β_EV265, increased ATP synthase and hydrolysis activity above that observed with XL10. Although the polar γT273H mutation is putatively capable of forming a hydrogen bond to β_EV265, its molecular volume (118 Å^3) is significantly larger than that of the wild-type residue threonine (93 Å^3), or the aspartate (91 Å^3) and asparagine (96 Å^3) mutants. This may explain the decreased ATP synthesis and hydrolysis activity of γT273H and the decrease in susceptibility to Mg^{2+}-ADP−AlF_n inhibition.

The results presented here show that the βP262G mutation decreases the extent of ATP synthase-dependent growth by 2-fold, virtually eliminates ATPase-dependent proton pumping and ATPase activity catalyzed by purified F_1, and decreases the sensitivity of the residual ATPase activity to inhibition by the Mg^{2+}-ADP−AlF_n species. However, the βP262A mutant was very similar to XL10 in almost every measured parameter. This proline of the PSAV segment reinforces the rigid sleeve that provides a link between the γT273−βV265 hydrogen bond and the Walker homology B βD256 and βR260 residues at the catalytic site. The ϕ and ψ angles of βP262 are not unusual and should be easily attained by either the βP262G or βP262A mutation, suggesting that the loss of activity of βP262G does not result from a forced change in the position of βV265. The low ATPase activity of βP262G-F_1 results from a large increase in the entropy of activation relative to the change in $\Delta H^{\ddagger}$. This suggests that this mutant causes a large increase in the number of possible conformations that could result from increased flexiblity in the sleeve.

Mutations in which prolines, alanines, and glycine were inserted into the hinge region of the Fe−S subunit of the bc_1 complex (*42*, *43*) were found to change the flexibility of the hinge in a manner similar to that of the alanine and glycine mutants reported here. In the bc_1 complex, the Fe−S head domain moves via a rotation of ∼55° and a translation greater than 15 Å. The proline and alanine mutations decreased hinge flexibility, while the glycine mutations increased the flexibility of this region. In the bc_1 complex, as in the PSAV segment of the β subunit, maintaining the appropriate level of flexibility was critical for function.

The results presented here strongly suggest that the hydrogen bond between β_{DP}V265 (MF_1V279) and γE275 (MF_1E261) is important for ATPase activity. The mutations that eliminate the hydrogen bond resulted in the largest decreases in ATPase activity. Mutations γE275G (48 Å^3) and γE275A (67 Å^3) that were smaller than the wild type (109 Å^3) had a greater effect on ATPase activity than the larger γE275V (105 Å^3) and γE275L (124 Å^3) substitutions. The effect of γE275K on membrane ATPase (*16*) was similar to the results of the mutants reported here that are unable to form a hydrogen bond. Mutations γE275D and γE275H that retained the ability to form a hydrogen bond to β_{DP}V265 had the highest ATPase activity. In the Mg^{2+}-ADP−AlF_n inhibition studies presented here, F_1 was preincubated with 1 molar equiv of ADP, which would allow the formation of only one Mg^{2+}-ADP−AlF_n molecule per F_1. A crystal structure of F_1 that contains only one Mg^{2+}-ADP−AlF_3 molecule has been determined (*2*). This structure closely resembles the ground state structure of Figure 1a, and lacks a hydrogen bond between γE275 and βV265. This may explain the lack of correlation between the susceptibility to Mg^{2+}-ADP−AlF_n inhibition and the ATPase activity of the γE275 mutants presented here.

The energy stored in the tightly wound conformation of the coiled coil present in the $(ADP{\cdot}AlF_4^-)_2F_1$ structure may contribute to the rate-limiting product release step since the γE275−β_EV265 hydrogen bond is only present in this structure, and mutations presented here that eliminate this hydrogen bond decrease ATPase activity by 2−3-fold. In the free energy plot (Figure 5), all γE275 mutants reported here decreased $\Delta H^{\ddagger}$ and $T\Delta S^{\ddagger}$. This type of compensation is characteristic of changes in the rate-limiting step of the reaction that result in fewer required bond rearrangements to complete the catalytic cycle. Although the rate-limiting step is more easily achieved because of the lower enthalpy of activation, the increased entropic component suggests that there is a large increase in the number of possible conformations introduced by the mutation. The slower observed rate of the reaction may then result from the increased time needed to attain a conformation that would allow the reaction to proceed. Similar results were also observed for mutations of βP262 and γT273.

The effects of the mutations reported here on the lactate-dependent proton gradient formation and on apparent ATP synthase activity are consistent with their possible participation in the escapement mechanism (*12*, *24*). In this mechanism, the transmembrane proton gradient provides constant torque to the γ subunit via the c subunit ring. However, the sum of hydrogen bonds and salt bridges between the γ

subunit and the $(\alpha\beta)_3$ subunit ring prevents rotation until the empty catalytic site binds substrate. As a result of substrate binding-dependent disruption of several γ subunit−$(\alpha\beta)_3$ ring interactions, the proton gradient-generated torque on the γ subunit exceeds the energy in the remaining hydrogen bonds and salt bridges, such that the γ subunit rotates. Rotation of the γ subunit induces the conformational changes in the catalytic sites necessary for ATP synthesis. Hydrophobic mutations to γT273 examined here decreased the proton gradient generated by lactate, suggesting that the membranes were not as tightly coupled as observed with the XL10 membranes. Membranes with charged or polar mutations to γT273 were more tightly coupled than the membranes that contained the hydrophobic mutations. These results are anticipated if the γT273−βV265 hydrogen bond contributes to the escapement mechanism.

Mutations that remove the γT273−βV265 hydrogen bond involved in the escapement mechanism might be expected to increase ATP hydrolysis activity. However, the k_{cat} of F_1 ATPase activity of the hydrophobic mutants reported here was significantly lower than that of XL10 F_1. The lower ATPase activity may result if these $\beta-\gamma$ subunit interactions also contribute to the mechanism that converts ATP binding and hydrolysis into rotational motion of the γ subunit. The Coulombic potential generated as γT273 comes within 5 Å of βV265 could contribute to an inductive force to drive γ subunit rotation (Figure 1A → Figure 1B). These interactions would need to work in concert with other similar $\beta-\gamma$ subunit interactions that come into van der Waals contact at different rotational positions of the γ subunit. Molecular modeling of the γ subunit rotation does support this hypothesis (Spetzler, Barber, and W. D. Frasch, unpublished results), though more experiments are required to determine further how many other γ subunit−$(\alpha\beta)_3$ ring interactions contribute significantly to the function of the enzyme.

ACKNOWLEDGMENT

We thank David S. Lowry for technical support, insightful discussions, and collaboration in the development of methods, and Laura Rodriguez for technical support.

REFERENCES

1. Abrahams, J. P., Leslie, A. G., Lutter, R., and Walker, J. E. (1994) Structure at 2.8 Å resolution of F1-ATPase from bovine heart mitochondria, *Nature 370*, 621−628.
2. Braig, K., Menz, R. I., Montgomery, M. G., Leslie, A. G., and Walker, J. E. (2000) Structure of bovine mitochondrial F_1-ATPase inhibited by Mg^{2+} ADP and aluminium fluoride, *Structure 8*, 567−573.
3. Noji, H., Yasuda, R., Yoshida, M., and Kinosita, K., Jr. (1997) Direct observation of the rotation of F1-ATPase, *Nature 386*, 299−302.
4. Sabbert, D., Engelbrecht, S., and Junge, W. (1996) Intersubunit rotation in active F-ATPase, *Nature 381*, 623−625.
5. Duncan, T. M., Bulygin, V. V., Zhou, Y., Hutcheon, M. L., and Cross, R. L. (1995) Rotation of subunits during catalysis by *Escherichia coli* F1-ATPase, *Proc. Natl. Acad. Sci. U.S.A. 92*, 10964−10968.
6. O'Neal, C. C., and Boyer, P. D. (1984) Assessment of the rate of bound substrate interconversion and of ATP acceleration of product release during catalysis by mitochondrial adenosine triphosphatase, *J. Biol. Chem. 259*, 5761−5767.
7. Yasuda, R., Noji, H., Yoshida, M., Kinosita, K., Jr., and Itoh, H. (2001) Resolution of distinct rotational substeps by submillisecond kinetic analysis of F1-ATPase, *Nature 410*, 898−904.
8. Yasuda, R., Noji, H., Kinosita, K., Jr., and Yoshida, M. (1998) F1-ATPase is a highly efficient molecular motor that rotates with discrete 120° steps, *Cell 93*, 1117−1124.
9. Yasuda, R., Noji, H., Yoshida, M., Kinosita, K., and Itoh, H. (2001) Resolution of distinct rotational substeps by submillisecond kinetic analysis of F-1-ATPase, *Nature 410*, 898−904.
10. Miki, J., Maeda, M., Mukohata, Y., and Futai, M. (1988) The γ-subunit of ATP synthase from spinach chloroplasts. Primary structure deduced from the cloned cDNA sequence, *FEBS Lett. 232*, 221−226.
11. Hong, S., and Pedersen, P. L. (2003) ATP synthases: Insights into their motor functions from sequence and structural analyses, *J. Bioenerg. Biomembr. 35*, 95−120.
12. Greene, M. D., and Frasch, W. D. (2003) Interactions among γ R268, γ Q269, and the β subunit catch loop of *Escherichia coli* F1-ATPase are important for catalytic activity, *J. Biol. Chem. 278*, 51594−51598.
13. Chen, W., Hu, C. Y., Crampton, D. J., and Frasch, W. D. (2000) Characterization of the metal binding environment of catalytic site 1 of chloroplast F1-ATPase from *Chlamydomonas*, *Biochemistry 39*, 9393−9400.
14. Ahmad, Z., and Senior, A. E. (2004) Mutagenesis of residue β-Arg-246 in the phosphate-binding subdomain of catalytic sites of *Escherichia coli* F1-ATPase, *J. Biol. Chem. 279*, 31505−31513.
15. Muller, M., Panke, O., Junge, W., and Engelbrecht, S. (2002) F1-ATPase, the C-terminal end of subunit γ is not required for ATP hydrolysis-driven rotation, *J. Biol. Chem. 277*, 23308−23313.
16. Iwamoto, A., Miki, J., Maeda, M., and Futai, M. (1990) H^+-ATPase γ subunit of *Escherichia coli*. Role of the conserved carboxyl-terminal region, *J. Biol. Chem. 265*, 5043−5048.
17. Sokolov, M., Lu, L., Tucker, W., Gao, F., Gegenheimer, P. A., and Richter, M. L. (1999) The 20 C-terminal amino acid residues of the chloroplast ATP synthase γ subunit are not essential for activity, *J. Biol. Chem. 274*, 13824−13829.
18. Nakamoto, R. K., al-Shawi, M. K., and Futai, M. (1995) The ATP synthase γ subunit. Suppressor mutagenesis reveals three helical regions involved in energy coupling, *J. Biol. Chem. 270*, 14042−14046.
19. Nakamoto, R. K., Maeda, M., and Futai, M. (1993) The γ subunit of the *Escherichia coli* ATP synthase. Mutations in the carboxyl-terminal region restore energy coupling to the amino-terminal mutant γ Met-23→Lys, *J. Biol. Chem. 268*, 867−872.
20. van Raaij, M. J., Abrahams, J. P., Leslie, A. G., and Walker, J. E. (1996) The structure of bovine F1-ATPase complexed with the antibiotic inhibitor aurovertin B, *Proc. Natl. Acad. Sci. U.S.A. 93*, 6913−6917.
21. Abrahams, J. P., Buchanan, S. K., Van Raaij, M. J., Fearnley, I. M., Leslie, A. G., and Walker, J. E. (1996) The structure of bovine F1-ATPase complexed with the peptide antibiotic efrapeptin, *Proc. Natl. Acad. Sci. U.S.A. 93*, 9420−9424.
22. Orriss, G. L., Leslie, A. G., Braig, K., and Walker, J. E. (1998) Bovine F1-ATPase covalently inhibited with 4-chloro-7-nitrobenzofurazan: The structure provides further support for a rotary catalytic mechanism, *Structure 6*, 831−837.
23. Menz, R. I., Walker, J. E., and Leslie, A. G. (2001) Structure of bovine mitochondrial F_1-ATPase with nucleotide bound to all three catalytic sites: Implications for the mechanism of rotary catalysis, *Cell 106*, 331−341.
24. Chen, W., and Frasch, W. D. (2001) Interaction of the catch-loop tyrosine β Y317 with the metal at catalytic site 3 of *Chlamydomonas* chloroplast F1-ATPase, *Biochemistry 40*, 7729−7735.
25. Senior, A. E., Latchney, L. R., Ferguson, A. M., and Wise, J. G. (1984) Purification of F1-ATPase with impaired catalytic activity from partial revertants of *Escherichia coli* uncA mutant strains, *Arch. Biochem. Biophys. 228*, 49−53.
26. Kato, Y., Sasayama, T., Muneyuki, E., and Yoshida, M. (1995) Analysis of time-dependent change of *Escherichia coli* F1-ATPase activity and its relationship with apparent negative cooperativity, *Biochim. Biophys. Acta 1231*, 275−281.
27. Dou, C., Grodsky, N. B., Matsui, T., Yoshida, M., and Allison, W. S. (1997) ADP-fluoroaluminate complexes are formed cooperatively at two catalytic sites of wild-type and mutant $\alpha_3\beta_3\gamma$ subcomplexes of the F-1-ATPase from the thermophilic *Bacillus* PS3, *Biochemistry 36*, 3719−3727.
28. Al-Shawi, M. K., and Senior, A. E. (1988) Complete kinetic and thermodynamic characterization of the unisite catalytic pathway of *Escherichia coli* F1-ATPase. Comparison with mitochondrial F1-ATPase and application to the study of mutant enzymes, *J. Biol. Chem. 263*, 19640−19648.

29. Futai, M., Sternweis, P. C., and Heppel, L. A. (1974) Purification and properties of reconstitutively active and inactive adenosinetriphosphatase from *Escherichia coli*, *Proc. Natl. Acad. Sci. U.S.A. 71*, 2725−2729.
30. Gibson, F., Downie, J. A., Cox, G. B., and Radik, J. (1978) Mu-induced polarity in the unc operon of *Escherichia coli*, *J. Bacteriol. 134*, 728−736.
31. Exner, O. (1973) The enthalpy−entropy relationship, *Prog. Phys. Org. Chem. 10*, 411−482.
32. Al-Shawi, M. K., Polar, M. K., Omote, H., and Figler, R. A. (2003) Transition state analysis of the coupling of drug transport to ATP hydrolysis by P-glycoprotein, *J. Biol. Chem. 278*, 52629−52640.
33. Allison, W. S., Ren, H., and Dou, C. (2000) Inhibitory Mg-ADP−Fluoroaluminate Complexes Bound to Catalytic Sites of F1-ATPases: Are They Ground-State or Transition-State Analogs? *J. Bioenerg. Biomembr. 32*, 531−538.
34. Nadanaciva, S., Weber, J., and Senior, A. E. (1999) Binding of the transition state analog MgADP-fluoroaluminate to F1-ATPase, *J. Biol. Chem. 274*, 7052−7058.
35. Gibbons, C., Montgomery, M. G., Leslie, A. G., and Walker, J. E. (2000) The structure of the central stalk in bovine F_1-ATPase at 2.4 Å resolution, *Nat. Struct. Biol. 7*, 1055−1061.
36. Menz, R. I., Leslie, A. G., and Walker, J. E. (2001) The structure and nucleotide occupancy of bovine mitochondrial F_1-ATPase are not influenced by crystallisation at high concentrations of nucleotide, *FEBS Lett. 494*, 11−14.
37. Weber, J., Wilke-Mounts, S., Lee, R. S., Grell, E., and Senior, A. E. (1993) Specific placement of tryptophan in the catalytic sites of *Escherichia coli* F1-ATPase provides a direct probe of nucleotide binding: Maximal ATP hydrolysis occurs with three sites occupied, *J. Biol. Chem. 268*, 20126−20133.
38. Weber, J., Hammond, S. T., Wilke-Mounts, S., and Senior, A. E. (1998) Mg^{2+} coordination in catalytic sites of F1-ATPase, *Biochemistry 37*, 608−614.
39. Lobau, S., Weber, J., Wilke-Mounts, S., and Senior, A. E. (1997) F1-ATPase, roles of three catalytic site residues, *J. Biol. Chem. 272*, 3648−3656.
40. Frasch, W. D. (2000) The participation of metals in the mechanism of the F_1-ATPase, *Biochim. Biophys. Acta 1458*, 310−325.
41. Hu, C. Y., Chen, W., and Frasch, W. D. (1999) Metal ligation by Walker homology B aspartate βD262 at site 3 of the latent but not activated form of the chloroplast F_1-ATPase from *Chlamydomonas reinhardtii*, *J. Biol. Chem. 274*, 30481−30486.
42. Darrouzet, E., Valkova-Valchanova, M., and Daldal, F. (2000) Probing the role of the Fe−S subunit hinge region during Q_o site catalysis in *Rhodobacter capsulatus* bc_1 complex, *Biochemistry 39*, 15475−15483.
43. Darrouzet, E., Valkova-Valchanova, M., Moser, C. C., Dutton, P. L., and Daldal, F. (2000) Uncovering the [2Fe2S] domain movement in cytochrome bc_1 and its implications for energy conversion, *Proc. Natl. Acad. Sci. U.S.A. 97*, 4567−4572.
44. Guex, N., and Peitsch, M. C. (1997) SWISS-MODEL and the Swiss-PdbViewer: An environment for comparative protein modeling, *Electrophoresis 18*, 2714−2723.

BI050070O